The Effect of the 18.6-Year Lunar Nodal Cycle on Steric Sea Level Changes

Sterre V Bult, Dewi Le Bars, Ivan D Haigh, Theo Gerkema

Geophysical Research Letters

RESEARCH LETTER
10.1029/2023GL106563

The Effect of the 18.6-Year Lunar Nodal Cycle on Steric Sea Level Changes

Sterre V. Bult[1,2], Dewi Le Bars[1], Ivan D. Haigh[3], and Theo Gerkema[4]

[1]Royal Netherlands Meteorological Institute (KNMI), De Bilt, The Netherlands, [2]Rijkswaterstaat, Utrecht, The Netherlands, [3]School of Ocean and Earth Science, University of Southampton, Southampton, UK, [4]Department of Estuarine and Delta Systems, NIOZ Royal Netherlands Institute for Sea Research, Yerseke, The Netherlands

Key Points:

- Steric sea level changes are influenced by the 18.6-year lunar nodal cycle along the western European coast
- This influence could result from the modulation of semidiurnal tides by the lunar nodal cycle and the associated change in ocean mixing
- This finding is a step toward resolving the long-standing discrepancy between the theoretical long-period nodal tide and observed signal

Supporting Information:

Supporting Information may be found in the online version of this article.

Correspondence to:

S. V. Bult,
S.V.Bult@tudelft.nl

Citation:

Bult, S. V., Le Bars, D., Haigh, I. D., & Gerkema, T. (2024). The effect of the 18.6-year lunar nodal cycle on steric sea level changes. *Geophysical Research Letters*, *51*, e2023GL106563. https://doi.org/10.1029/2023GL106563

Received 26 SEP 2023
Accepted 21 MAR 2024

Abstract We show that steric sea-level varies with a period of 18.6 years along the western European coast. We hypothesize that this variation originates from the modulation of semidiurnal tides by the lunar nodal cycle and associated changes in ocean mixing. Accounting for the steric sea level changes in the upper 400 m of the ocean solves the discrepancy between the nodal cycle in mean sea level observed by tide gauges and the theoretical equilibrium nodal tide. Namely, by combining the equilibrium tide with the nodal modulation of steric sea level, we close the gap with the observations. This result supports earlier findings that the observed phase and amplitude of the 18.6-year cycle do not always correspond to the equilibrium nodal tide.

Plain Language Summary The orbital position of the moon and the gravity pull it exerts on the earth varies with a period of 18.6 years. This cycle is called the lunar nodal cycle and it results in small variations of yearly averaged sea level (~1–2 cm). Understanding this variability is important because it allows, for example, to quickly detect an acceleration in local sea-level rise due to global warming. Here we show that the lunar nodal cycle also has an influence on the temperature and salinity in the surface 400m of the ocean. As a result, the ocean density changes and amplifies sea level variations along the western European coast. We make the hypothesis that since the lunar nodal cycle also influences the amplitude of the semidiurnal tides, and since those tides are known to be responsible for a large part of ocean mixing, a change in ocean mixing could be the cause of the ocean density variability that we observe.

1. Introduction

The 18.6-year lunar nodal cycle, the precession of the lunar ascending node, produces the main modulation of the tidal range on decadal timescales (Pugh, 1987). Therefore, this cycle is important when considering inter-annual variations in extreme sea level events and coastal flooding. The nodal modulation of the tidal range amounts to up to 30 cm in different locations around the world (Enriquez et al., 2022; Haigh et al., 2011; Peng et al., 2019; Thompson et al., 2021). The spatial variations in the amplitude and phase of the nodal modulations depend on the tidal characteristics, for example, diurnal or semidiurnal (Haigh et al., 2011). Theoretically, the nodal modulation has an effect of 3.7% on the semidiurnal M2 tide, which is a first approximation. The effect is relatively larger on the diurnal tides, K1 and O1, namely 11% and 19% (Pugh, 1987). The observed tide is generally not exactly equal to the equilibrium tide, as the formulation does not take into account the dynamic response of the oceans to the tidal forces. The equilibrium theory (i.e., assuming the constituents conform to the tide-generating potential) seems to overpredict the nodal modulation of the semidiurnal M2 tide in several regions of the world (Feng et al., 2015; Pineau-Guillou et al., 2021). It has been argued that the differences can be partly explained by the effects of friction and resonance (Ku et al., 1985). Other studies that have reported discrepancies are Ray (2006), who reported values between 2.3% and 3.6% in the Gulf of Maine, and Müller (2011), who showed relative amplitudes between 1.3% and 3.9%.

The nodal cycle is not only observed in the tidal range but also in mean sea level. The theoretical equilibrium nodal tide has a maximum amplitude at the poles, zero amplitude at °±°35°N, is out-of-phase between poles and equator and has no zonal dependence, much like a standing wave (Proudman, 1960). The amplitude increases with about 25% when accounting for loading and self-attraction (Agnew & Farrell, 1978; Woodworth, 2012). Multiple studies have observed the nodal tide in mean sea level time-series from tide gauge records across the globe (Cherniawsky et al., 2010; Iz, 2006; Lisitzin, 1974; Rossiter, 1967). Recently, research has found that the nodal cycle can influence estimates of sea level rise acceleration (Houston & Dean, 2011; Keizer et al., 2023).

However, the observed phase and amplitude do not always seem to correspond to the equilibrium tide, which may be partly due to a contamination of the signal with other multi-decadal oscillations (e.g., ocean-atmosphere internal variability), as suggested by Woodworth (2012).

The question as to what extent the nodal tide—the long-period oscillation of mean sea level—follows the equilibrium tide is thus still unresolved. Up to now, this question has been considered as detached from the other nodal effect, the 18.6 years modulation of the tidal range and the associated modulation of tidal current amplitudes. In this paper, we propose a possible connection between the two, via a long-period modulation of tidal mixing and associated steric sea level changes. Internal tides have a large influence on diapycnal mixing in the ocean (Garrett & St. Laurent, 2002; Munk & Wunsch, 1998; Vic et al., 2019). Internal tides are generated when tidal waves encounter rough topography, such as mid-ocean ridges and continental shelves (Polzin et al., 1997). They are a significant source term for the power input to the oceanic internal wavefield (Waterhouse, et al., 2014).

The influence of the nodal cycle on diapycnal mixing was hypothesized by Loder and Garrett (1978), who used a model of vertical mixing showing significant variation in sea surface temperature (SST). McKinnell and Crawford (2007) showed a significant cross-correlation of the air temperature record and SSTs with the lunar nodal cycle. Bi-decadal oscillations of SST were attributed to the nodal modulation of the high frequency tides (Osafune & Yasuda, 2006), and the modified SST may be amplified through a midlatitude air-sea interaction (Osafune et al., 2014). Recently, Joshi et al. (2023) suggested that not only the SST, but also salinity and temperature at depth vary with the nodal cycle. This implies that the density varies with the nodal cycle as well.

Interestingly, Frederikse et al. (2016), while closing the sea level budget for the Northwestern European continental shelf, concluded that the observed nodal cycle follows the equilibrium law, which is in apparent contradiction with Keizer et al. (2023). However, Frederikse et al. (2016) considered the signal that is left after having removed the effect of steric variations (as well as wind effects and mass changes) on sea level. We argue in this paper that steric sea level changes are responsible for the observed discrepancy between the 18.6-year cycle observed from tide gauges along the western European coast and the equilibrium lunar nodal tide.

2. Data

2.1. Tide Gauges

Yearly averaged mean sea-level measurements are used from 14 tide gauges along the European coast, namely: Cascais, Brest, Newlyn, Vlissingen, Hoek van Holland, IJmuiden, Den Helder, Harlingen, Delfzijl, Cuxhaven, Esbjerg, North Shields, Stavanger and Bergen (Figure 1a). These stations are chosen because their temporal coverage includes at least five nodal cycles. In addition, they have few data gaps. The data before 1890 was discarded for all tide gauges to avoid the inclusion of a sea-level jump around 1885 (Baart et al., 2019; Frederikse & Gerkema, 2018).

2.2. Temperature and Salinity

Two analysis products for temperature and salinity data are used, namely EN4.2.2 (Good et al., 2013) with bias correction from Gouretski and Franco (2010) and IAP (Cheng et al., 2017). The data sets contain objective analyses from the temperature and salinity data. Both data sets are gridded at a $1° \times 1°$ horizontal resolution. The vertical resolution varies with depth with a higher resolution close to the surface than at depth. The EN4 data set covers the period 1900 to present and has 42 depth levels going down to over 5000m water depth, while IAP provides data from 1940 to present covering 41 depth levels down to a depth of 2000m.

2.3. Atmospheric Reanalysis

The monthly mean zonal and meridional wind at 10m from two atmospheric reanalysis products are used. The ERA5 reanalysis is available from 1940 to present (Hersbach et al., 2023), and has a spatial resolution of $0.25° \times 0.25°$. The second product, the Twentieth Century Reanalysis Version 3 (20CRv3) is available from 1836 to 2015 (Slivinski et al., 2019), with a spatial resolution of $1.0° \times 1.0°$.

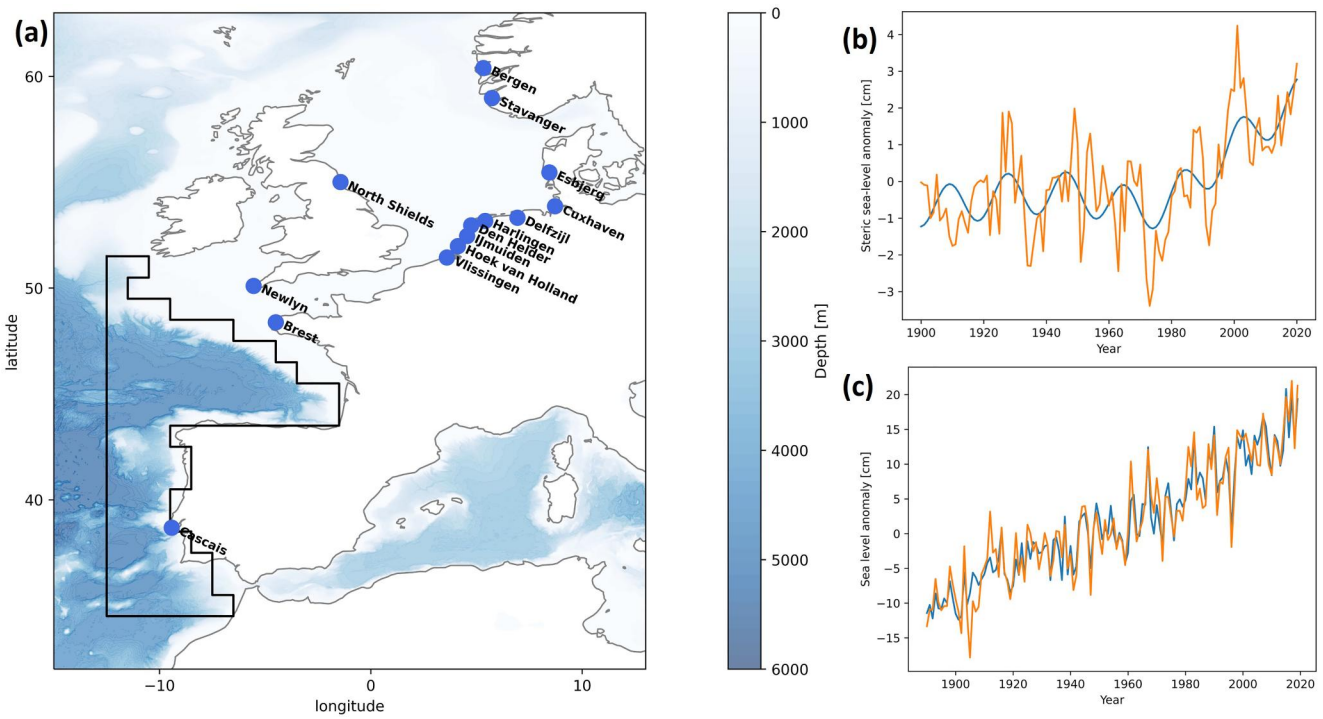

Figure 1. (a) Location of the 14 tide gauges used to determine the nodal modulation in the mean sea level along the European coast and the region of steric sea level integration, that we call extended Bay of Biscay. The bathymetry is shown in the background. (b) Annual steric sea-level anomaly averaged over the extended Bay of Biscay (orange) and Generalized Additive Model (GAM) model fit including a long-term trend and a sinusoidal with a period of 18.6 years (blue). (c) Annual sea level anomaly for the tide gauge of Delfzijl (orange) and GAM model fit including a long-term trend, wind effects, and a sinusoidal with a period of 18.6 years (blue).

3. Method

3.1. Equilibrium Tide

The phase and the amplitude of the theoretical equilibrium tide for each location are determined using the equation provided by Woodworth (2012), which is based on Agnew and Farrell (1978). We assume that the amplitude approximates the self-consistent equilibrium law, accounting for self-attraction and loading (Richter et al., 2013), by including the factor $L = 1.2$ in Equation 1, and that the phase does not shift (Woodworth, 2012). The period is 18.61 years, with the reference set at 1922.7. High extremes close to the poles occur at the same time as low extremes along the equator, with a latitude of separation at $\pm$ 35.3°N. The amplitude is dependent on the latitude as well, with the maximum amplitude at the poles:

$$n = A\,cos\left(\frac{2\pi(t-1922.7)}{18.61}+\pi\right) \quad \text{with} \quad A = A_e L(1+k_2-h_2)\left(3\,\sin^2\theta-1\right) \tag{1}$$

Where n is the surface displacement due to the nodal cycle, $k_2 = 0.298$,$h_2 = 0.6032$ and the amplitude A is expressed in cm; time t is measured in years and latitude θ is expressed in radians. The parameters k_2 and h_2 are Love numbers and are included to account for the change in potential and elastic response of the solid Earth. The amplitude at the equator A_e is 0.88 cm (Table 1 from Woodworth (2012)).

3.2. Determining the Nodal Signal

To estimate the nodal cycle from the observations, a statistical model called Generalized Additive Model (GAM) is used (Hastie & Tibshirani, 2017; Wood, 2020). This model is like a multi-linear regression with the added benefit that it is not necessary to make assumptions on the shape of the trend. For the annual averaged tide gauge data the model includes a trend, a sinusoidal function with free amplitude and phase at the period of the nodal cycle, and zonal and meridional wind stress (Keizer et al., 2023). The wind stress is included via terms

$\sqrt{u^2+v^2} * u$ and $\sqrt{u^2+v^2} * v$, where u and v are the zonal and meridional wind from the reanalysis. Wind from the nearest reanalysis grid box from the tide gauges are used in the regression model. To model steric sea-level change, we do not include wind since there is no direct physical mechanism relating them. The model fit to steric sea level change and one tide gauge are shown in Figures 1b and 1c.

3.3. Steric Sea Level Changes

Ocean density is computed from temperature and salinity data using the GSW-Python toolbox (TEOS-10, 2017), a python implementation of the Thermodynamic Equation of Seawater 2010 (TEOS-10). Subsequently, steric sea level changes are derived. Steric sea-level changes on the continental shelf are negligibly small because it is shallow. However, those in the deep ocean are felt on the shallow shelf areas by mass transfer (Landerer et al., 2007). The choice for the appropriate deep-sea region and depth of integration of steric sea-level change to estimate the influence of steric sea-level change on tide gauge measurements was discussed in Bingham & Hughes, (2012). Here we choose the region of the extended Bay of Biscay (Figure 1a) which has a strong correlation with sea-level variability in the North Sea (Frederikse et al., 2016). Frederikse et al. (2016) also showed that satellite altimetry observations indicate a coherence between the North Sea and the Norwegian coast. Therefore, for all tide gauge stations, we assume that the steric sea-level changes are equal to those of the extended Bay of Biscay. As we go back in time the quality and quantity of temperature and salinity observations reduces. We find that using steric sea-level data for the period 1960–2020 and integrating to a depth of 400m provides the best fit with tide gauge observations (see Supporting Information S1).

4. Results

We fit the GAM including a trend and a sinusoidal function with free amplitude and phase at the period of the nodal cycle to each point of the steric sea-level change data set to obtain the spatial variation of the phase and magnitude (Figures 2a and 2b). For a large region from Northern Morocco to Ireland the nodal cycle in the steric sea-level peaks around 2002 (Figure 2a). To compare steric sea level-change to tide gauges, we compute the difference between the nodal cycle estimated from the observed sea level signal and the equilibrium tide at each tide gauge station. This provides an estimate of the non-equilibrium tide at the tide gauges. We see that for all tide gauges the phase of the maximum is around 2002, like in the region of the extended Bay of Biscay, even though local steric sea-level changes are different. North of Scotland a sharp shift occurs, with a peak around 2004 in the Atlantic Ocean, while the cycle in the Norwegian Sea peaks around 1995. The regions are therefore out-of-phase.

The amplitude of the nodal modulation in the steric sea-level changes (Figure 2b) is small in the region North of Scotland, where the phase is shifted. This might be due to the North Atlantic Current impinging on the shelf and advecting steric anomalies away (Daniault et al., 2016). The amplitude is larger in the extended Bay of Biscay, about 1 cm. The amplitudes at the tide gauges surrounding the North Sea are in the range of the amplitude in the steric sea-level changes in the extended Bay of Biscay. However, the amplitudes in the shallow areas indicated by the 400 m isobath, such as the northwest European shelf, are smaller. Thus, the local steric sea-level changes are not reflected in the tide gauge observations, but rather the amplitude in the steric sea-level changes in the deep sea. The results for both phase and magnitude of the estimated steric sea-level changes at the tide gauges support the choice of the extended Bay of Biscay at the region influencing the most the mass transport to the western European shelves resulting from steric sea-level changes.

To assess whether the period of the nodal cycle is dominant in the observed signal of steric sea-level changes in the extended Bay of Biscay, we compute the spatially averaged steric sea-level in that region and apply the GAM model with varying periods of the sinusoidal signal. We find that the amplitudes are largest around 18.6 years (Figure 2c). This points toward the nodal cycle as the dominant multi-year cycle and makes it unlikely that the observed signal would be the result of internal ocean-atmosphere variability.

The amplitude and phase of the different nodal cycle components (observed signal, equilibrium tide, steric signal, sum of steric and equilibrium signal) at each tide gauge are shown in Figures 2d and 2e. The amplitude of the equilibrium tide increases with latitude and is smaller than the observed nodal amplitude at all tide gauges. The equilibrium tide only overlaps with the uncertainty range of observed nodal cycle in Bergen. The nodal modulation of the steric sea-level changes is the same for all tide gauges, as it is equal to the steric sea level changes of the extended Bay of Biscay. The steric amplitude agrees more closely with the observed amplitude. Adding the

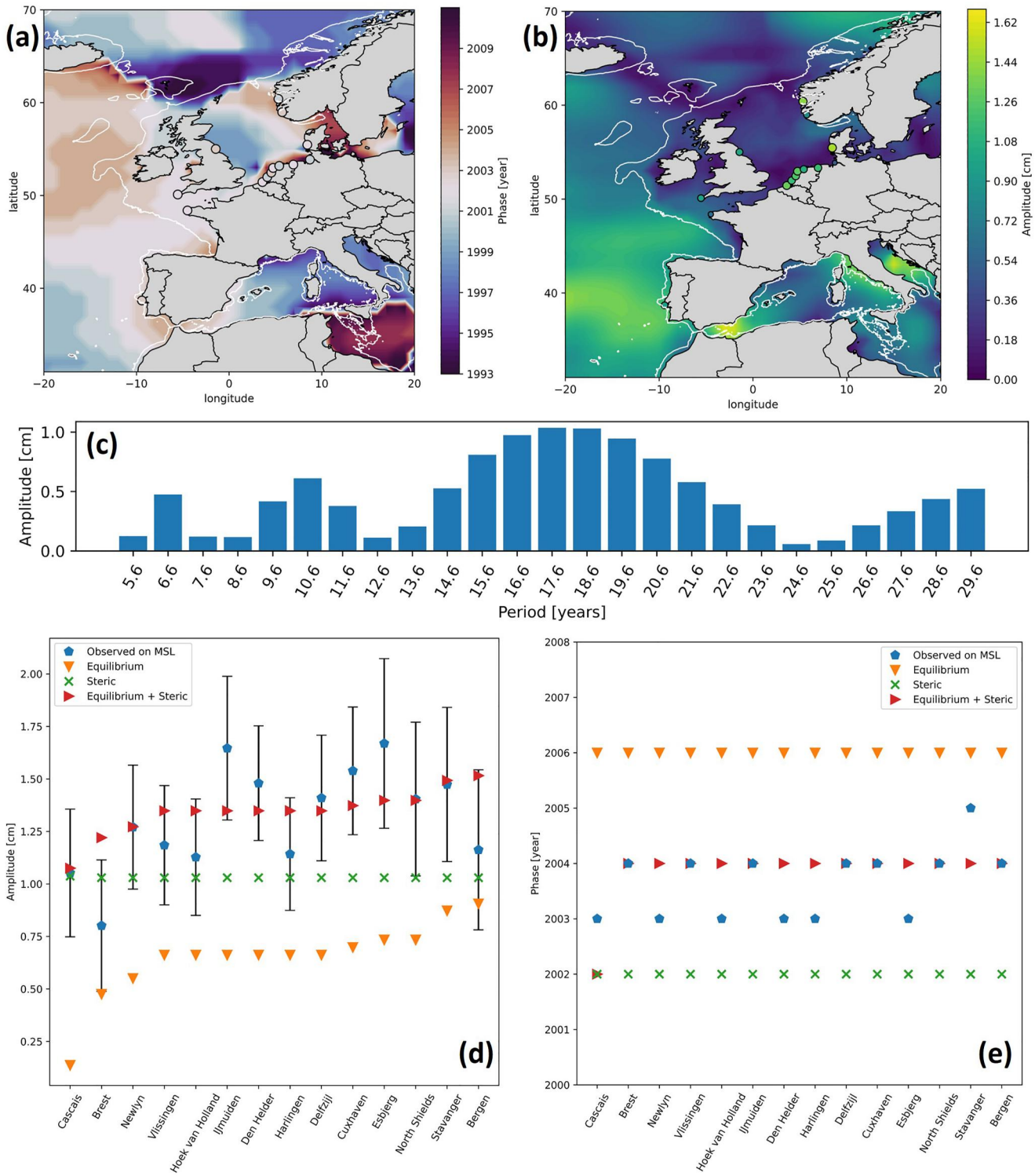

Figure 2. (a) Phase and (b) amplitude of the nodal modulation in the steric sea level changes integrated over the top 400m of the ocean for the EN4 data set post-1960. The white lines represent the 400m isobath. The phase is defined as the year when the sinusoidal signal reaches a maximum between 1993 and 2011. The dots indicate the phase (a) and amplitude (b) of the observed sea level minus the equilibrium tide at the tide gauges. (c) Amplitude of the sinusoidal function through the steric sea level changes for different periods expressed in years for the EN4 data set post-1960. (d) Amplitudes and (e) phase of the different components of the nodal cycle for the 14 tide gauges post-1890. The observed amplitudes include error bars representing ±1 standard deviation in the estimation of the nodal cycle from the tide gauge data. The standard deviation for the estimation of the steric amplitude is 0.13 cm. The average error in the observed phase is 0.87 years (0.62–1.42 years). Because the phase is annually resolved, the error bars are not shown. MSL stands for Mean Sea Level in the legends of panels d and (e).

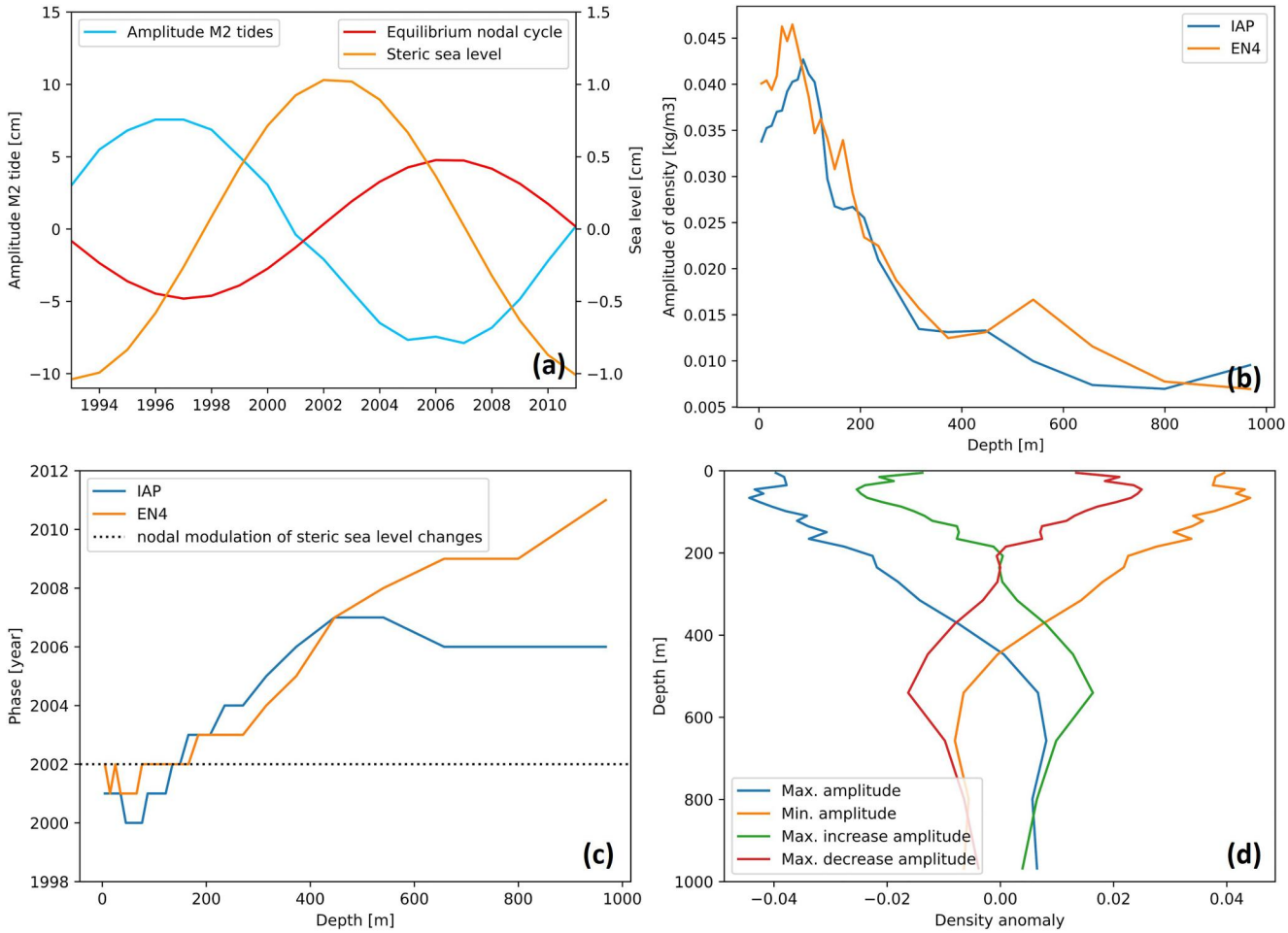

Figure 3. (a) Amplitude anomaly of the M2 tide in Brest from Pineau-Guillou et al. (2021), equilibrium nodal tide in Brest and modulation in the steric sea level changes in the extended Bay of Biscay. (b) Amplitude and (c) phase of the nodal cycle in the density for water depths between 0 and 1000m for the EN4 and IAP data sets. (d) Density anomaly in kg/m^3 at four instances of the nodal modulation of steric sea level changes between 0 and 1000m water depth for the EN4 data set.

steric and equilibrium components results in most cases in an amplitude close to the observed amplitude. The sum is outside the observed uncertainty range only for Brest. The equilibrium tide peaks in 2006, while the observed nodal cycle peaks in 2003 or 2004 for most tide gauge stations (Figure 2e). The nodal modulation in the steric sea-level change on the other hand peaks earlier, in 2002. The sum of the steric and equilibrium nodal signals falls approximately in the middle and approaches the phase of the observed signal better than the steric or equilibrium nodal cycle for most tide gauges.

From the phase of the different components of the nodal cycle, it was apparent that the peak of the nodal steric component precedes the peak of the equilibrium nodal tide. This can be clearly seen in Figure 3a. The nodal steric leads the equilibrium tide by approximately 4 years. The M_2 tide is dominant in this region and its range varies with the nodal cycle (Pineau-Guillou et al., 2021) as shown in Figure 3a for the tide gauge of Brest. It is in opposition of phase with the equilibrium tide, peaking around 1997. The effect of the nodal modulation on the M_2 tide at Brest is ±4.3% (Pineau-Guillou et al., 2021). The modulation in the steric sea level changes is in quadrature with the modulation in the tides, it increases when the amplitude of tides is larger than average, while the opposite occurs when the amplitude of tides is smaller than average.

Up to now we have considered steric sea level changes, which integrate density anomalies vertically, but the effect of the nodal cycle on the density varies with depth (Figure 3b). The amplitude in the density is largest in the top 400m of the water column, with a peak in amplitude around 50–100m water depth. The difference in amplitude between the EN4 and IAP data sets is small. The phase of the nodal cycle influence on density also varies with

depth. Near the surface, the nodal signal in the density peaks around 2001, while at 400m water depth the peak occurs around 2005 (Figure 3c). Deeper than 400m depth there is a discrepancy between EN4 and IAP possibly because of a lack of data before the deployment of Argo floats.

We now look at vertical density profiles at different stages of the nodal cycle (Figure 3d). The density is smallest at the moment of a maximum of steric sea level changes in the top 400m, while there is a small positive anomaly for the deeper layers. The opposite is the case for the moment of a minimum amplitude, where in the upper layers the density is largest. At the moment of a maximum increase in the steric sea level, which corresponds with the largest amplitude in M2 tides, there is a negative anomaly in the top 200m and a positive one in the deeper water columns. This could be an indication of increased vertical mixing.

5. Conclusion and Discussion

We used observational data to determine the effect of the lunar nodal cycle on steric mean sea level changes. The results show that there is a nodal modulation of steric mean sea level changes in the extended Bay of Biscay. This is linked to the nodal modulation of the semi-diurnal tides and, presumably, the associated changes in tidal mixing. We argue that the nodal modulation of steric sea level combines with the equilibrium nodal cycle at the western European coast by showing that their sum agrees more closely with the observed nodal cycle than the equilibrium nodal tide alone. This confirms the findings of earlier research that concluded that the observed nodal cycle does not follow the equilibrium tide (Keizer et al., 2023). Accounting for the steric sea level changes, as was done by Frederikse et al. (2016), closes the gap with the observed nodal cycle, thus resolving the discrepancy.

We propose that the observed nodal modulation of steric sea-level changes is a result of changes in tidal mixing. The amplitude of M2 tides and steric sea level are in quadrature. This is because the time scale of adjustment of the ocean temperature and salinity is longer than the time scale of the variability in mixing. A useful analogy to understand this lag is the relation between solar irradiance and ocean heat content during the annual cycle. In the North Atlantic the solar irradiance is maximum in June but the maximum ocean heat content is in September due to the large thermal inertia of the ocean (Gleckler et al., 2006). The vertical diffusion variation due to the nodal cycle and the ocean heat content was also found to be approximately in quadrature by Joshi et al. (2023). The mechanism described in Joshi et al. (2023) for the global ocean is that increased vertical diffusion reduces the sea surface temperature and increases ocean heat flux from the atmosphere to the ocean. This is consistent with Loder and Garrett (1978) who found a reduction in sea surface temperature in phase with maximum tidal mixing along the coasts of the United States. For our region of interest, the extended Bay of Biscay, the physical link between the nodal modulation of the amplitude of M2 tides and steric sea level in the surface 400m of the ocean is not straight forward because both temperature and salinity are contributing to the changes in density (Figure SM3 in Supporting Information S1). In this area the important water mass is the Eastern North Atlantic Central Water (ENACW) which is formed between the subtropical and subpolar gyres during winter subduction (Liu & Tanhua, 2021). However, some processes on the continental shelf also have an influence on the ENACW in the Bay of Biscay. Gómez-Gesteira et al. (2013) report the importance of winter deep mixing between Brest and Ireland and van Aken (2001) shows the importance of diapycnal mixing along the shelf break for the salinity of this water mass. Those processes could be influenced by more energetic M2 tides either through stronger tidal currents or breaking internal waves. For a more detailed understanding on where buoyancy is entering the ocean and how it reaches the Bay of Biscay, numerical computations with a regional ocean model would be needed (Akpinar et al., 2020).

The mechanism we propose here for the western European coast cannot be directly generalized to other regions. One of the limiting factors to determine the observed nodal cycle is the availability of long tide gauge records. Another reason why the mechanism cannot be observed consistently in other regions of the world might be the presence of ocean currents (Talley et al., 2011). In the extended Bay of Biscay, the presence of strong ocean currents is limited, as the North Atlantic Current deflects toward the north and south near the edge of the northwest European shelf (Daniault et al., 2016). The local density anomalies remain relatively unaffected, and the small nodal signal can be detected. This is not the case for most other coastal systems. For example, along the Japanese coast the Kuroshio current is strong and the combined signal at the tide gauges in that region does not approach the observed nodal signal well. However, we found two other tide gauges for which the mechanism we propose seem to also be at work. At the Pensacola tide gauge, in the Gulf of Mexico, the observed nodal cycle is approached relatively well by adding the steric and equilibrium signals. This might be due to the weaker current further into the Gulf. Another location is the Ketchikan tide gauge. This tide gauge lays approximately between

the Alaska Current and the California Current System therefore the steric sea-level changes might be relatively unaffected by these two current systems.

Data Availability Statement

All data and code necessary to reproduce the results presented in this paper are openly available. The tide gauge data was obtained from the Permanent Service for Mean Sea Level (Holgate et al., 2013; PSMSL, 2023). EN.4.2.2 data are available in Met Office Hadley Centre (2023), Good et al. (2013) describe how the data set was constructed. The IAP data is available from Cheng et al. (2017) for temperature and Cheng et al. (2020) for salinity. Surface winds from ERA5 are available from Hersbach et al. (2023) and the twentieth Century Reanalysis data is available at PSL (2023). The ETOPO2 data is available at NOAA National Centers for Environmental Information (2022). The code used to produce the results described in this paper is available on GitHub at Bult and Le Bars (2023) under the GNU General Public License v3.

Acknowledgments
The authors would like to thank Lucia Pineau-Guillou for providing the data of the amplitude of the M2 tide at the tide gauge of Brest and Aslak Grinsted for early brainstorming about the ideas presented in this paper. This publication was supported by PROTECT. This project has received funding from the European Union's Horizon 2020 research and innovation program (Grant 869304), PROTECT contribution number 92.

References

Agnew, D. C., & Farrell, W. E. (1978). Self-consistent equilibrium ocean tides. *Geophysical Journal of the Royal Astronomical Society*, *55*(1), 171–181. https://doi.org/10.1111/j.1365-246x.1978.tb04755.x

Akpinar, A., Charria, G., Theetten, S., & Vandermeirsch, F. (2020). Cross-shelf exchanges in the northern Bay of Biscay. *Journal of Marine Systems*, *205*, 103314. https://doi.org/10.1016/j.jmarsys.2020.103314

Baart, F., Rongen, G., Hijma, M., Kooi, H., de Winter, R., & Nicolai, R. (2019). Zeespiegelmonitor 2018: De stand van zaken rond de zeespiegelstijging langs de Nederlandse kust. Retrieved from https://deltalife.deltares.nl/deltares/de_nederlandse_delta/zeespiegelstijging/160368/Zeespiegelmonitor_2018_final.pdf

Bingham, R. J., & Hughes, C. W. (2012). Local diagnostics to estimate density-induced Sea Level variations over topography and along coastlines: Topography and SEA LEVEL. *Journal of Geophysical Research*, *117*, C1. https://doi.org/10.1029/2011JC007276

Bult, S. V., & Le Bars, D. (2023). Code and data for "The effect of the 18.6-year lunar nodal cycle on steric sea level changes. Retrieved from https://github.com/KNMI-sealevel/CodeNodalCyclePaper

Cheng, L., Trenberth, K., Fasullo, J., Boyer, T., Abraham, J., & Zhu, J. (2017). Improved estimates of ocean heat content from 1960 to 2015. *Science Advances*, *3*, e1601545. https://doi.org/10.1126/sciadv.1601545

Cheng, L., Trenberth, K. E., Gruber, N., Abraham, J. P., Fasullo, J., Li, G., et al. (2020). Improved estimates of changes in upper ocean salinity and the hydrological cycle. *Journal of Climate*, *33*(23), 10357–10381. https://doi.org/10.1175/JCLI-D-20-0366.1

Cherniawsky, J. Y., Foreman, M. G., Kang, S. K., Scharroo, R., & Eert, A. J. (2010). 18.6-year lunar nodal tides from altimeter data. *Continental Shelf Research*, *30*(6), 575–587. https://doi.org/10.1016/j.csr.2009.10.002

Daniault, N., Mercier, H., Lhermninier, P., Sarafanov, A., Falina, A., Zunino, P., et al. (2016). The northern North Atlantic Ocean mean circulation in the early 21 st century. *Progress in Oceanography*, *146*, 142–158. https://doi.org/10.1016/j.pocean.2016.06.007

Enriquez, A. R., Wahl, T., Baranes, H., Talke, S. A., Orton, P. M., Booth, J. F., & Haigh, I. D. (2022). *Predictable changes in extreme sea levels and coastal flood risk due to nodal and perigean astronomical tidal cycles*. Authorea. https://doi.org/10.1002/essoar.10508511.1

Feng, X., Tsimplis, M. N., & Woodworth, P. L. (2015). Nodal variations and long-term changes in the main tides on the coasts of China. *Journal of Geophysical Research: Oceans*, *120*(2), 1215–1232. https://doi.org/10.1002/2014jc010312

Frederikse, T., & Gerkema, T. (2018). Multi-decadal variability in seasonal mean sea level along the North Sea coast. *Ocean Science*, *14*(6), 1491–1501. https://doi.org/10.5194/os-14-1491-2018

Frederikse, T., Riva, R., Kleinherenbrink, M., Wada, Y., van den Broeke, M., & Marzeion, B. (2016). Closing the sea level budget on a regional scale: Trends and variability on the northwestern european continental shelf. *Geophysical Research Letters*, *43*(10), 864–872. https://doi.org/10.1002/2016GL070750

Garrett, C., & St. Laurent, L. (2002). Aspects of deep ocean mixing. *Journal of Oceanography*, *58*(1), 11–24. https://doi.org/10.1023/a:1015816515476

Gleckler, P. J., Sperber, K. R., & AchutaRao, K. (2006). Annual cycle of global ocean heat content: Observed and simulated. *Journal of Geophysical Research*, *111*(C6), C06008. https://doi.org/10.1029/2005JC003223

Gómez-Gesteira, M., de Castro, M., Santos, F., Álvarez, I., & Costoya, X. (2013). Changes in ENACW observed in the Bay of Biscay over the period 1975–2010. *Continental Shelf Research*, *65*(August), 73–80. https://doi.org/10.1016/j.csr.2013.06.014

Good, S. A., Martin, M. J., & Rayner, N. A. (2013). EN4: Quality controlled ocean temperature and salinity profiles and monthly objective analyses with uncertainty estimates. *Journal of Geophysical Research: Oceans*, *118*(12), 6704–6716. https://doi.org/10.1002/2013JC009067

Gouretski, V., & Franco, R. (2010). On depth and temperature biases in bathythermograph data: Development of a new correction scheme based on analysis of a global ocean database. *Deep Sea Research Part I: Oceanographic Research Papers*, *57*(6), 812–833. https://doi.org/10.1016/j.dsr.2010.03.011

Haigh, I. D., Eliot, M., & Pattiaratchi, C. (2011). Global influences of the 18.61 year nodal cycle and 8.85 year cycle of lunar perigee on high tidal levels. *Journal of Geophysical Research*, *116*(C6), C06025. https://doi.org/10.1029/2010JC006645

Hastie, T. J., & Tibshirani, R. J. (2017). *Generalized additive models*. Routledge. https://doi.org/10.1201/9780203753781

Hersbach, H., Bell, B., Berrisford, P., Biavati, G., Horányi, A., Muñoz Sabater, J., et al. (2023). ERA5 hourly data on pressure levels from 1940 to present. *Copernicus Climate Change Service (C3S) Climate Data Store (CDS)*. https://doi.org/10.24381/cds.bd0915c6

Holgate, S. J., Matthews, A., Woodworth, P. L., Rickards, L. J., Tamisiea, M. E., Bradshaw, E., et al. (2013). New data systems and products at the permanent Service for Mean Sea Level. *Journal of Coastal Research*, *29*, 493–504. https://doi.org/10.2112/JCOASTRES-D-12-00175.1

Houston, J. R., & Dean, R. G. (2011). Accounting for the nodal tide to improve estimates of sea level acceleration. *Journal of Coastal Research*, *27*(5), 801–807. https://doi.org/10.2112/jcoastres-d-11-00045.1

Iz, B. (2006). How do unmodeled systematic mean sea level variations affect long-term sea level trend estimates from tide gauge data? *Journal of Geodesy*, *80*(1), 40–46. https://doi.org/10.1007/s00190-006-0028-x

Joshi, M., Hall, R. A., Stevens, D. P., & Hawkins, E. (2023). The modelled climatic response to the 18.6-year lunar nodal cycle and its role in decadal temperature trends. *Earth System Dynamics*, *14*(2), 443–455. https://doi.org/10.5194/esd-14-443-2023

Keizer, I., Le Bars, D., de Valk, C., Jüling, A., van de Wal, R., & Drijfhout, S. (2023). *The acceleration of sea-level rise along the coast of The Netherlands started in the 1960s*. EGUsphere. https://doi.org/10.5194/egusphere2022-935

Ku, L.-F., Greenberg, D. A., Garrett, C. J. R., & Dobson, F. W. (1985). Nodal modulation of the lunar semidiurnal tide in the Bay of Fundy and Gulf of Maine. *Science*, *230*(4721), 69–71. https://doi.org/10.1126/science.230.4721.69

Landerer, F. W., Jungclaus, J. H., & Marotzke, J. (2007). Ocean bottom pressure changes lead to a decreasing length-of-day in a warming climate. *Geophysical Research Letters*, *34*(6), L06307. https://doi.org/10.1029/2006GL02910

Lisitzin, E. (1974). *Sea-level changes*, Elsevier Scientific Publishing Company, 286.

Liu, M., & Tanhua, T. (2021). Water masses in the Atlantic Ocean: Characteristics and distributions. *Ocean Science*, *17*(2), 463–486. https://doi.org/10.5194/os-17-463-2021

Loder, J. W., & Garrett, C. (1978). The 18.6-year cycle of sea surface temperature in shallow seas due to variations in tidal mixing. *Journal of Geophysical Research*, *83*(C4), 1967–1970. https://doi.org/10.1029/jc083ic04p01967

McKinnell, S. M., & Crawford, W. R. (2007). The 18.6-year lunar nodal cycle and surface temperature variability in the northeast Pacific. *Journal of Geophysical Research*, *112*(C2), C02002. https://doi.org/10.1029/2006JC003671

Met Office Hadley Centre. (2023). EN4: Quality controlled subsurface ocean temperature and salinity profiles and objective analyses. [Dataset]. Retrieved from https://www.metoffice.gov.uk/hadobs/en4/

Müller, M. (2011). Rapid change in semi-diurnal tides in the North Atlantic since 1980. *Geophysical Research Letters*, *38*(11), L11602. https://doi.org/10.1029/2011GL047312

Munk, W. H., & Wunsch, C. (1998). Abyssal recipes II: Energetics of tidal and wind mixing. *Deep-Sea Research Part I*, *45*(12), 1977–2010. https://doi.org/10.1016/S0967-0637(98)00070-3

NOAA National Centers for Environmental Information. (2022). ETOPO 2022 15 arc-second global relief model. [Dataset]. *NOAA National Centers for Environmental Information*. https://doi.org/10.25921/fd45-gt74

Osafune, S., Masuda, S., & Sugiura, N. (2014). Role of the oceanic bridgein linking the 18.6 year modulation of tidal mixing and long-term SST change in the North Pacific. *Geophysical Research Letters*, *41*(20), 7284–7290. https://doi.org/10.1002/2014GL061737

Osafune, S., & Yasuda, I. (2006). Bidecadal variability in the intermediate waters of the northwestern subarctic Pacific and the Okhotsk Sea in relation to 18.6-year period nodal tidal cycle. *Journal of Geophysical Research*, *111*(C5). https://doi.org/10.1029/2005JC003277

Peng, D., Hill, E. M., Meltzner, A. J., & Switzer, A. D. (2019). Tide gauge records show that the 18.61-year nodal tidal cycle can change high water levels by up to 30 cm. *Journal of Geophysical Research: Oceans*, *124*(1), 736–749. https://doi.org/10.1029/2018JC014695

Permanent Service for Mean Sea Level (PSMSL). (2023). Tide gauge data. [Dataset]. *National Oceanography Centre*. Retrieved from http://www.psmsl.org/data/obtaining/

Physical Sciences Laboratory (PSL). (2023). NOAA/CIRES/DOE 20th century reanalysis (V3). [Dataset]. *National Oceanic and Atmospheric Administration Climate Program Office*, Retrieved from https://psl.noaa.gov/data/gridded/data.20thC_ReanV3.html

Pineau-Guillou, L., Lazure, P., & Wöppelmann, G. (2021). Large-scale changes of the semidiurnal tide along North Atlantic coasts from 1846 to 2018. *Ocean Science*, *17*, 17–34. https://doi.org/10.5194/os-17-17-2021

Polzin, K. L., Toole, J. M., Ledwell, J. R., & Schmitt, R. (1997). Spatial variability of turbulent mixing in the abyssal ocean. *Science*, *276*(5309), 93–96. https://doi.org/10.1126/science.276.5309.93

Proudman, J. (1960). The condition that a long-period tide shall follow the equilibrium law. *Geophysical Journal of the Royal Astronomical Society*, *3*(2), 244–249. https://doi.org/10.1111/j.1365-246x.1960.tb00392.x

Pugh, D. T. (1987). *Tides, surges and Mean Sea-level*. Wiley-Blackwell.

Ray, R. D. (2006). Secular changes of the M_2 tide in the Gulf of Maine. *Continental Shelf Research*, *26*(3), 422–427. https://doi.org/10.1016/j.csr.2005.12.005

Richter, K., Riva, R. E. M., & Drange, H. (2013). Impact of self-attraction and loading effects induced by shelf mass loading on projected regional sea level rise. *Geophysical Research Letters*, *40*(6), 1144–1148. https://doi.org/10.1002/grl.50265

Rossiter, J. R. (1967). An analysis of annual sea level variations in European waters. *Geophysical Journal of the Royal Astronomical Society*, *12*(3), 259–299. https://doi.org/10.1111/j.1365-246x.1967.tb03121.x

Slivinski, L. C., Compo, G. P., Whitaker, J. S., Sardeshmukh, P. D., Giese, B. S., McColl, C., et al. (2019). Towards a more reliable historical reanalysis: Improvements for version 3 of the twentieth century reanalysis system. *Quarterly Journal of the Royal Meteorological Society*, *145*(724), 2876–2908. https://doi.org/10.1002/qj.3598

Talley, L. D., Pickard, G. L., Emery, W. J., & Swift, J. H. (2011). *Descriptive physical oceanography: An introduction*(6th ed.). Elsevier, 560.

TEOS-10. (2017). GSW-Python. Retrieved from https://teos-10.github.io/GSW-Python/

Thompson, P. R., Widlansky, M. J., Hamlington, B. D., Merrifield, M. A., Marra, J. J., Mitchum, G. T., & Sweet, W. (2021). Rapid increases and extreme months in projections of United States high-tide flooding. *Nature Climate Change*, *11*(7), 584–590. https://doi.org/10.1038/s41558-021-01077-8

van Aken, H. M. (2001). The hydrography of the mid-latitude northeast Atlantic Ocean—Part III: The subducted thermocline water mass. *Deep Sea Research Part I: Oceanographic Research Papers*, *48*(1), 237–267. https://doi.org/10.1016/S0967-0637(00)00059-5

Vic, C., Naveira Garabato, A. C., Mattias Green, J. A., Waterhouse, A. F., Zhao, Z., Melet, A., et al. (2019). Deep-ocean mixing driven by small-scale internal tides. *Nature Communications*, *10*(1), 2099. https://doi.org/10.1038/s41467-019-10149-5

Waterhouse, A. F., MacKinnon, J. A., Nash, J. D., Alford, M. H., Kunze, E., Simmons, H. L., et al. (2014). Global patterns of diapycnal mixing from measurements of the turbulent dissipation rate. *Journal of Physical Oceanography*, *44*(7), 1854–1872. https://doi.org/10.1175/JPO-D-13-0104.1

Wood, S. N. (2020). Inference and computation with generalized additive models and their extensions. *Test*, *29*(2), 307–339. https://doi.org/10.1007/s11749-020-00711-5

Woodworth, P. L. (2012). A note on the nodal tide in sea level records. *Journal of Coastal Research*, *28*(2), 316–323. https://doi.org/10.2112/JCOASTRES-D-11A-00023.1

References From the Supporting Information

Cheng, L., & Zhu, J. (2016). Benefits of CMIP5 multimodel ensemble in reconstructing historical ocean subsurface temperature variation. *Journal of Climate*, *29*(15), 5393–5416. https://doi.org/10.1175/JCLI-D-15-0730.1

Dijkstra, H. A. (2008). Dynamical Oceanography. Springer Science & Business Media.

Roemmich, D., & Owens, W. B. (2000). The Argo Project: Global ocean observations for understanding and prediction of climate variability. *Oceanography*, *13*(2), 45–50. https://doi.org/10.5670/oceanog.2000.33